



STScI | SPACE TELESCOPE
SCIENCE INSTITUTE

Instrument Science Report COS 2025-19(v1)

Reference File Updates Following the Application of New Geometric Distortion and Walk Corrections II: TDSTAB and HVDSCORR

Jacqueline Hernandez¹, S. Hasselquist¹, W. Fischer¹, E. Frazer¹, D. French¹, N. Indriolo^{1,2}, C. I. Johnson¹, D. Kakkad^{1,3}, L. P. Miller¹, M. Rafelski¹, R. Sankrit¹

¹ Space Telescope Science Institute, Baltimore, MD

² AURA for European Space Agency, STScI, USA

³ Centre for Astrophysics Research, University of Hertfordshire, Hatfield AL10 9AB, UK

2 December 2025

ABSTRACT

We present updated time-dependent sensitivity (TDS) corrections for the far-ultraviolet (FUV) channel on board the Cosmic Origins Spectrograph (COS). Updated TDS corrections were required due to the recently derived geometric distortion, delta-geometric, X-walk, and Y-walk corrections introduced in the COS calibration pipeline. The new high-voltage-dependent sensitivity (HVDS) correction was also applied to all COS FUV data via the HVDSCORR module in CalCOS and incorporated into the TDS corrections. Monitoring data were binned in wavelength and fit using a piecewise linear function of time. The analysis included TDS monitoring data of calibrator white dwarfs from the start of monitoring in September 2009 until February 2024. Comparison of the recalibrated data with CALSPEC models WD0308-565 and GD71 showed that the time-dependent flux calibration is within the 5% absolute and 2% relative requirements for all FUV gratings. The residuals between data and model over time show 2-10% improvements across all wavelength bins for all Lifetime Positions (LPs).

Contents

1. Introduction	2
2. High Voltage Dependent Sensitivity Correction (HVDSCORR)	3
2.1 Introduction to HVDSCORR	4
2.2 HVDSCORR Improvements	4
3. TDS Data	5
4. TDS Methodology	7
4.1 Special Considerations	7
4.1.1 LP2 FLUXTAB Bug	7
4.1.2 G130M/1096/FUVB	8
4.1.3 G130M/1327/FUVA	9
4.1.4 G140L/1105/FUVA	9
4.1.5 G140L/800 and G160M/1533	9
5. Scientific Testing	9
6. Summary	10
Change History for COS ISR 2025-19	10
References	10
Appendix A	11

1. Introduction

The sensitivity of the Cosmic Origins Spectrograph (COS) far-ultraviolet (FUV) channel declines over time (Osten et al. 2010). Regular monitoring programs were established to follow any trends using calibrator white dwarf stars (Osten et al. 2011). The sensitivity is monitored at various wavelength bins for each combination of central wavelength (cenwave) and segment (FUVA, FUVB) and are used to correct for sensitivity loss. The corrections are stored in the time-dependent sensitivity (TDS) reference file, TDSTAB, and used in conjunction with the photometric throughput reference file, FLUXTAB, to obtain flux-calibrated data in the CalCOS pipeline.

The derivation of new geometric distortion and walk corrections (Indriolo et al. 2025a) altered the FUV detector coordinate system, leading to changes in the reported positions of photon events. Along with the updated reference files that define the new coordinate frame, reference files “downstream” in the CalCOS pipeline, such as the TDSTAB, required updating as well. New reference files were delivered with the updated geometric distortion and walk corrections as summarized in Indriolo et al. (2025b).

In addition to the new geometric distortion and walk corrections, a new

Table 1. Reference files replaced in CRDS

File Type	USEAFTER	Old File Name	LP	Current File Name
TDSTAB	11 May 2009	52m2056fl_tds.fits		97h18216l_tds.fits
	02 Oct 2017	83j20454l_tds.fits		
FLUXTAB	11 May 2009	62m1953bl_phot.fits	1	97h1819fl_phot.fits
	11 May 2009	62m1953cl_phot.fits	2	97h18182l_phot.fits
	02 Oct 2017	83j20457l_phot.fits	2	
	11 May 2009	62m19539l_phot.fits	3	97h1818ml_phot.fits
	02 Oct 2017	83j2044tl_phot.fits	3	
	11 May 2009	62m19537l_phot.fits	4	97h18177l_phot.fits
	02 Oct 2017	83j20455l_phot.fits	4	
	02 Oct 2017	83j20452l_phot.fits	5	97h18172l_phot.fits
	02 Oct 2017	83j20451l_phot.fits	6	

high-voltage dependent sensitivity (HVDS) correction was applied. The sensitivity of the COS detector slightly increases with increasing high voltage (HV), resulting in a $\sim 1\text{-}2\%$ change in sensitivity across the commanded HV levels typically used in COS observations (Sahnou et al. 2016). As discussed more in Section 2, the HVDS is a new step in CalCOS that applies a small correction to the weighted counts of all photon events to account for this. This correction is applied after the FLATCORR step in the calibration pipeline, several steps before extraction occurs.

Prior to this work, the COS team used two TDSTABs with two different USEAFTER dates with the more recent USEAFTER date being cenwave dependent (Sankrit & Rowlands 2021). Due to a lack of resources at the time and the expectation that older data would not change significantly, the COS team decided to “freeze” the TDS model of the former TDSTAB for data collected before 2 October 2017. During the creation of this new TDSTAB file described in this work, cenwave dependence was propagated backwards across the full history of COS, and we combined the two TDSTABs into a single cenwave-dependent TDSTAB. This also means that, for the LPs that contain observations across the 2017 USEAFTER date, we now only need a single FLUXTAB (see also Miller et al. 2025). In total, eleven reference files that were in use in CRDS were replaced with seven reference files (Table 1).

2. High Voltage Dependent Sensitivity Correction (HVDS CORR)

In addition to the new walk and geometric corrections, the CalCOS calibration code was modified to include an “HVDS CORR” module that applies a small sensitivity correction based on FUV detector high voltage, described in detail below and in Section 3.4.12 of the COS Data Handbook (Indriolo et al. 2025).

2.1 Introduction to HVDESCORR

As discussed in detail in Sahnou et al. (2016), the COS FUV detector exhibits an approximately linear correlation between detector sensitivity and detector HV, a phenomenon henceforth referred to as the high voltage dependent sensitivity (HVDS). Previous TDS analyses have noted increases in the “NET” count rate for exposures taken immediately after the HV is raised. The TDS does not explicitly account for these jumps in count rate, and therefore increases to the HV will induce small errors in the derived slopes of the TDS. Another consequence of not accounting for the HVDS is that exposures taken at the same time but at different HVs will yield inconsistent flux measurements.

To correct for the HVDS, we have implemented a simple linear correction in CalCOS that applies a scaling factor (SF) to the “EPSILON” column (weighted counts) of a corrtag events list based on the HV, defined explicitly as:

$$SF = c_1 \times (HV - HV_0) + 1$$

The HVDSTAB reference file contains the values of c_1 and HV_0 for each cenwave and each segment. While the HVDS is thought to primarily be a detector effect, the HVDSTAB is cenwave-dependent to allow for a more flexible application to the data in any potential cases where the TDS slopes for a specific cenwave may be even better fit with an HVDS correction of a slightly different magnitude than what was derived from the Sahnou et al. (2016) data (which only analyzed the HVDS for cenwaves G140L/1280, G130M/1291, and G160M/1623). For this recalibration effort, we adopt $c_1 = -0.001568$ and $HV_0 = 167$ for the FUV A, and $c_1 = -0.001373$ and $HV_0 = 169$ for the FUV B. Slopes (c_1) were derived by repeating the analysis of Sahnou et al. (2016) and measuring the slope of NET counts with commanded HV level using the PID 13971 data, which consisted of exposures of WD0308-565 taken at a wide range of HV values. The values of HV_0 were chosen to minimize the magnitude of the correction that would be applied to the maximum of exposures. As this is believed to be a detector effect the HVDESCORR correction to “EPSILON” is applied after the FLATCORR step in CalCOS, but before extraction and flux calibration occurs.

2.2 HVDESCORR Improvements

In general, the HVDS improves the linear TDS model (described in more detail in Section 4) across time periods during which the HV was increased. We show in Figure 1 how these increases in “NET” counts are generally improved for the new TDS (green) as compared to the old TDS (black) for G160M 1623 FUV A TDS observations. Specifically, “NET” increases across the date when the HV was raised (indicated by the vertical purple lines) are smaller or nonexistent for the new TDS as compared to the old TDS. We also show in Table 2 some more examples of how the slopes and uncertainties change across certain times with two or more HV increases. In general, the fractional

uncertainty is smaller for the new (“Current”) TDS, suggesting the HVDS results in slightly better fits. However, the sensitivity change from an HV increase is not always completely corrected, suggesting future efforts to understand potential time and detector location dependence of the HVDS might result in even larger improvements.

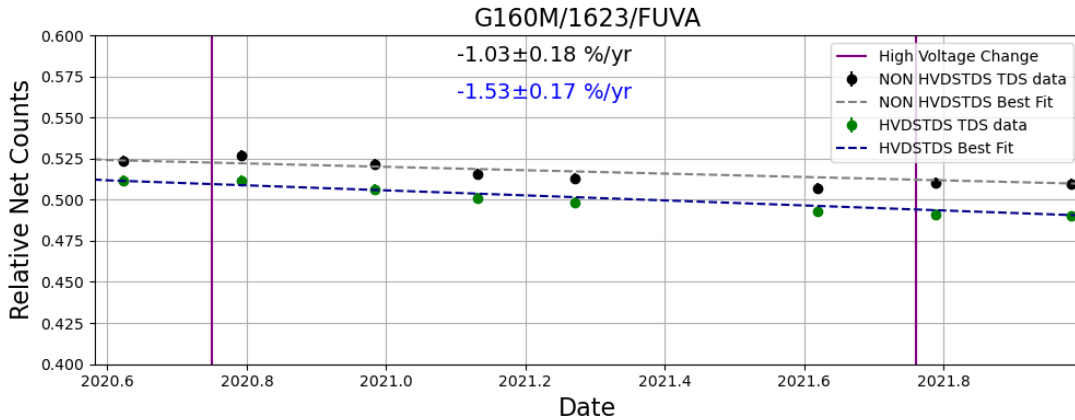


Figure 1. NET counts as a function of time for TDS observations of G160M cenwave 1623 FUVA across a time period over which there are two HV increases (indicated by the purple vertical lines). Points from the previous TDS are shown in black, and points from the new TDS with HVDS CORR applied are shown in green. Slopes across this range are indicated in black (old TDS) and blue (new TDS). As a byproduct of redoing the TDS for data pre-2017, whereas previously all TDS deliveries contained only data taken after 2017, the slopes are propagated to longer times, resulting in steeper values. In both cases, the slope reductions across HV changes are smaller for the new TDS, although a residual increase remains. The fractional uncertainty in the slope decreases with the new TDS, suggesting better overall TDS fits across this region.

To further demonstrate HVDS CORR improvements, we show in Figure 2 an observation of WD0308-565 that was inadvertently taken at a higher HV (175) than nominal during flux calibration at LP5. Cyan points denote the difference between binned flux and a model for the data as they were in MAST, with the old TDSTAB and before the HVDS CORR step was implemented, and green points show the same points for the data after correction with the new TDSTAB and HVDS CORR. Prior to this new TDS work, because the TDS data were taken at a lower HV (169), the FLUX TABs that were backed out could not account for this difference in HV, resulting in the cyan points being nearly 2% offset from the model. However, when HVDS CORR is applied along with the new TDSTAB, the flux of this observation is once again correct (green points).

3. TDS Data

Regular observations of flux calibration standard stars (WD0947+857, WD1057+719, GD71, WD0308-565) are obtained throughout the lifetime of COS using the shortest

Table 2. TDS slopes of a given mode and temporal breakpoint with multiple HV changes

Mode	Breakpoint	HV Changes	Old TDS Slope (%/yr)	Current TDS Slope (%/yr)
G130M/1291/FUVA	2013.8	167, 173, 167	-3.06 ± 0.08	-3.60 ± 0.08
G130M/1291/FUVB	...	169, 175, 163	-0.41 ± 0.10	-1.05 ± 0.10
G130M/1222/FUVA	2020.6	163, 167, 173	-0.29 ± 0.14	-1.11 ± 0.14
G130M/1222/FUVB	...	163, 169	-0.75 ± 0.55	-0.50 ± 0.53
G160M/1623/FUVA	...	163, 167, 173	-1.03 ± 0.18	-1.53 ± 0.17
G160M/1623/FUVB	...	163, 169	-0.73 ± 0.22	-1.41 ± 0.21

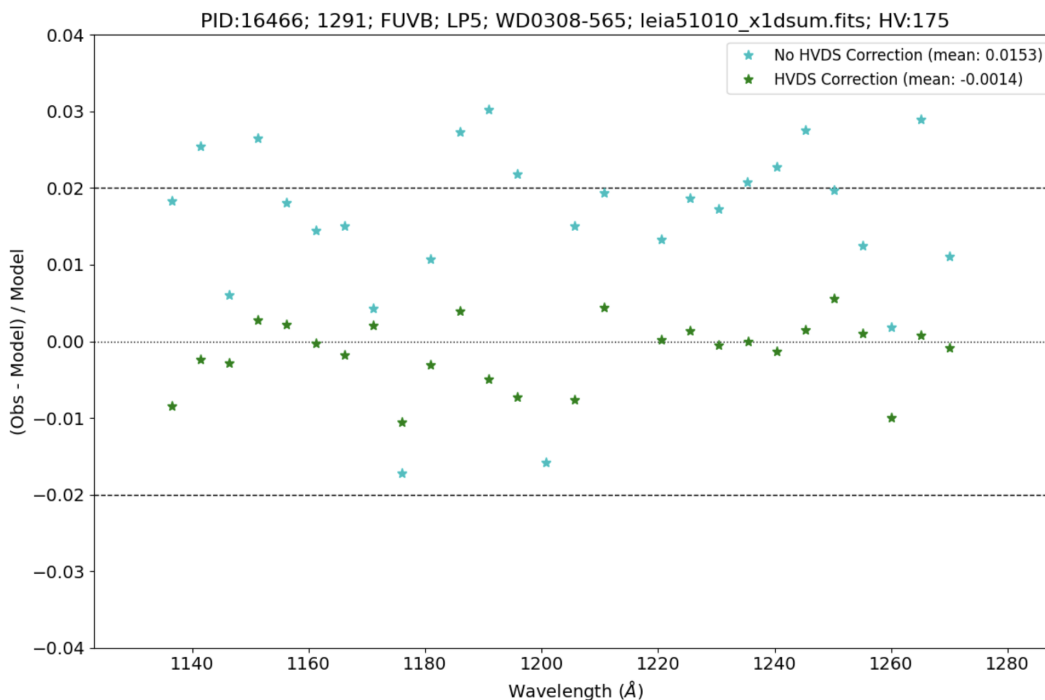


Figure 2. Observations of a dataset used to calibrate the LP5 FLUXTAB that highlights the previous incompatibility of the TDS and FLUXTAB at different HVs. The FLUXTAB observation was taken at HV = 175 whereas the TDS observation was taken at HV = 169. When the FLUXTABs were “backed out” following the old TDS derivation, this FLUXTAB observation was almost 2% offset from the model (cyan points). With the new TDSTAB and HVDSCORR applied, this exposure is once again consistent with the model (green points). The mean of both fits are listed in the legend.

and longest standard cenwave for each medium resolution grating and all available cenwaves for the low resolution grating. The cenwaves that are routinely observed

have been updated as cenwaves are retired and new observation modes are introduced. All of these observations are part of the COS FUV Spectroscopic Sensitivity Monitor program, an ongoing yearly calibration program that observes white dwarf standard stars at a 1-2 month cadence since September 2009. More information concerning these programs, which provide the data used in creating the TDSTAB, is provided in Table 3 and previous analysis documented in Osten et al. 2010 - 2012, Kriss et al. 2013, Roman-Duval et al. 2014 - 2015, Sana et al. 2015, de Rosa et al. 2016 - 2018, Sankrit 2019 - 2020, and Rowlands & Sankrit 2021 - 2024.

4. TDS Methodology

TDS monitoring data were calibrated with the updated reference files described in Indriolo et al. 2025b (along with the HVDSTAB described in Section 2), and intermediate FLUXTAB files produced as part of the FLATFILE/FLUXTAB analysis (Miller et al. 2025) for each LP, using CalCOS v3.6.0 with the TDSTAB delivered to CRDS in 2024 (83j204541_tds.fits) and 2021 (52m2056fl_tds.fits) as noted in Table 1. The data were processed using the TDS analysis described in Bostroem et al. (2015) and outlined here. The net count rate from x1d.fits are binned into 5 and 20 Å bins for the medium and low resolution modes, respectively, with the blue modes binned in 20 Å bins, except for G130M/1055/FUVB where 60 Å bins are used, to ensure a $S/N > 50$ per wavelength bin. Binned net counts are then scaled to the first monitoring exposure of each cenwave and segment combination and then scaled across LPs. A piecewise linear function is fit to each wavelength bin over time between breakpoints (Osten & Bostroem 2014, Bostroem et al. 2015). The piecewise linear function is forced to be equal at each break point.

The TDSTAB was created using the code described in Boestroem et al. 2014. Accompanying FLUXTABs for all LPs were derived using the generated TDSTAB in a process known as “backing out”. This process involves applying the newly derived TDS corrections to an absolute sensitivity curve of a given LP setting from the closest but lesser breakpoint date and calculates the drop in sensitivity. This sensitivity drop is then applied to create a finalized FLUXTAB. Because we initially derived the updated FLUXTABs using data with HVDCORR = ‘OMIT’, we also had to back out the HVDCORR correction (see e.g., Miller et al. 2025). The updated TDS slopes are shown in Figure 4 for the breakpoint early in 2023.

4.1 Special Considerations

4.1.1 LP2 FLUXTAB Bug

Because of a bug in how the FLUXTAB reference files are derived from the TDSTAB, introduced when the TDSTAB changed from grating-dependent to cenwave-dependent (Sankrit & Rowlands 2021), the FUVB segment of the observational modes

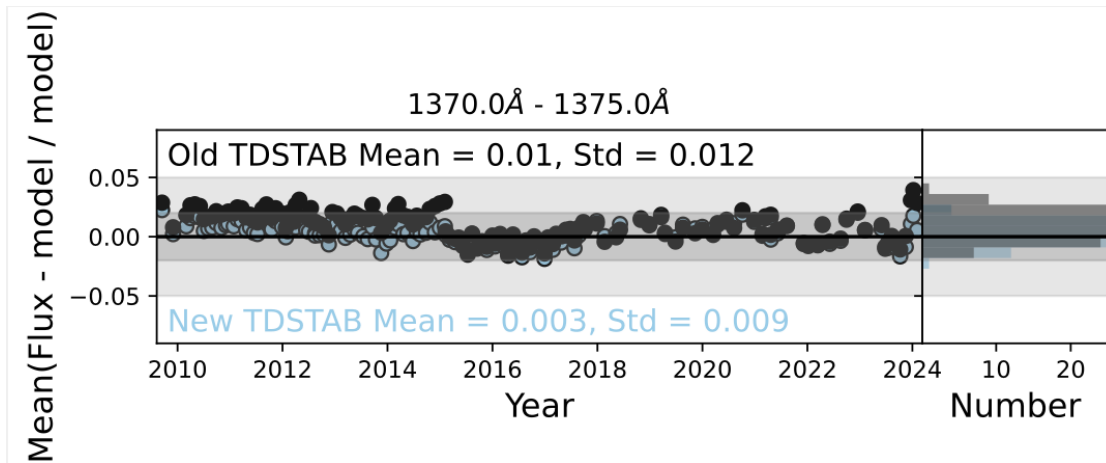


Figure 3. The FUV TDS slopes (percentage change per year) as a function of wavelength for the TDSTAB creation, for each grating and segment (see legend). Uncertainties on the slopes are small at most wavelengths, but are larger near the detector edges and around airglow lines.

G130M/1055 and G130M/1096, colloquially known as the "Blue Modes", was previously uncorrected by the TDS. This bug was rectified by modifying how the FLUXTAB is derived for LP2 Blue Modes. We manually moved the breakpoint used in this method from 5 September 2013 to 20 October 2013. In addition, we removed Blue Mode data between 19 September 2012 and 20 October 2013 to accommodate the modification, as data during this time period experienced little to no loss in sensitivity.

4.1.2 G130M/1096/FUVB

In calibrating the G130M/1096/FUVB exposures, the wavelength bin 1010 - 1030 Å increased in sensitivity beginning March 2023. No other wavelength bin showed similar behavior. This false increase is due to absorption lines present in the wavelength bin which the gainsag table (97h18184l_gsag.fits) flagged as gain sagged and omitted. Currently, the false increase does not affect the derived TDS model.

To address this, we modified the TDS code for this setting and use the dq_wgt array from a February 2024 exposure (lf4g04b6q_x1d.fits; PID 17326) and applied it to all exposures for all time. By holding the dq_wgt array fixed, the false increase disappears. For now, the dq_wgt array will remain fixed for all previous and future exposures of this setting.

4.1.3 G130M/1327/FUVA

The bluest edge of G130M/1327/FUVA, around 1325 Å, shows the net count rate much lower in the calibration with the current reference files than with the previous calibration. The S/N of this region is lower compared to the rest of the segment and leads to more scatter as a result. We removed the first three 5 Å bins of this setting to improve the overall S/N of the region and allow the created TDSTAB to extrapolate a correction based on the remainder of the segment. This improves the TDS fit in this edge.

4.1.4 G140L/1105/FUVA

The reddest edge of G140L/1105/FUVA, >1950 Å, shows a poorer calibration in the TDSTAB that has been derived using the new reference files. This may be due to overall poor calibration of wavelength regions greater than 1950 Å due to second order light contamination which the new calibration accentuated further (Hirschauer, A. S. et al. 2024). This is a known issue in COS/FUV. We decided to make no modifications for this setting because the flux calibration is uncertain at these wavelengths.

4.1.5 G140L/800 and G160M/1533

Historically, the TDSTAB included data from the G140L/800 Flux Calibration and Cross Dispersion Profile program (PI R. Sankrit; PID 15483) and the G160M/1533 Profiles and Fluxes program (PI E. Frazer; PID 15458) to correspond to settings' first exposure in time. However, these exposures (ldso01ioq for G140L/800, ldsi51kaq for G160M/1533/FUVA, and ldsi02u2q for G160M/1533/FUVB) are on the MAST Do-Not-Reprocess list and required manual calibration in order to be included. These exposures were omitted from the TDSTAB creation.

5. Scientific Testing

We calibrated all TDS monitoring data with the final TDSTAB and FLUXTABs, alongside the reference files described in Indriolo et al. 2025b, to provide the final flux calibration. To assess accurate flux calibration, we analyze the extent to which there are residual flux offsets between the TDS observations and CALSPEC models across time and wavelength. To perform the comparisons, the data and model are binned in wavelength using the same size bins as used to create the TDSTAB, described above.

Using the new TDSTAB and associated reference files described in Indriolo et al. 2025b, residuals between observations and model are comparable to or show significant improvements over the data calibrated with the previous CRDS reference files, with residuals improving by 2 - 10%. In the highly used mode G130M/1291, the FUVA segment showed consistent improvements throughout all LPs (Figures 4 and 5). We

also verified that the new TDSTAB successfully removed some large residuals that were present in the previous TDSTAB, as shown in Figure 6. For most observing modes at most LPs, the mean of the residuals is typically centered around zero and in most wavelength bins meets our absolute flux calibration goal of 5%. These improvements were most notable at the segment edges for the new reference files.

We also calibrated TDS monitoring data not included in creating the new TDSTAB to test the reference file. These observations were from PID 17326 and 17328 and range from May 2024 to January 2025 for all monitored modes. In general, there were significant improvements between the data calibrated with the old and new TDSTAB (Figures 7, 8, 9, and 10).

6. Summary

Monitoring data of the white dwarfs WD0947+857, WD1057+719, WD0308-565, and GD71 were recalibrated with new reference files described in Indriolo et al. 2025b and the new HVDSTAB reference file. A piecewise linear function was used to derive updated TDS corrections for all settings at all LPs since monitoring began. The updated TDSTAB and FLUXTABs were tested by calibrating all TDS monitoring data both included in the creation of the TDSTAB and not included, providing a 2% - 10% improvement in the overall flux calibration. The largest improvement due to the new reference files are shown in the segment edges while the HVDS yields improvements across the entire wavelength range. Flux offsets due to wavelength and time were removed and the flux calibration is within the 5% absolute and 2% relative calibration requirements. The TDSTAB (97h18216l.tds.fits) and subsequent FLUXTABs were delivered to CRDS reference-file database on July 2025. The two USEAFTER dates of 11 May 2009 and 2 October 2017 were removed for this delivery to have a single USEAFTER date of 11 May 2009 for the TDSTAB and FLUXTABs.

Change History for COS ISR 2025-19

Version 1: 2 December 2025- Original Document

References

- Bostroem, K. A., et al. 2015, COS Technical Instrument Reports 2014-05
- Bohlin, R. C., Gordon, K. D., & Tremblay, P. E. 2014, Publications of the Astronomical Society of the Pacific, 126, 711-732. doi:10.1086/677655
- Bohlin, R. C., Hubeny, I., & Rauch, T. 2020, Astronomical Journal, 160, 21. doi:10.3847/1538-3881/ab94b4
- Hirschauer, A. S. et al. 2024, Cosmic Origins Spectrograph Instrument Handbook, Version 17.0 (Baltimore: STScI)
- Indriolo, N., Ake, T., Debes, J., et al. 2025a, COS ISR 2025-07

Indriolo, N., Fischer, W., Frazer, E., et al. 2025b, COS ISR 2025-08
Indriolo, N., et al. 2025, COS Data Handbook, Version 6.0, (Baltimore: STScI).
Kriss, G. A., et al. 2013, COS Instrument Science Report 2013-04
Miller, L. P. et al. 2025, COS Instrument Science Report 2025-12
Osten, R. A., et al. 2010, COS Instrument Science Report 2010-15
Osten, R. A., et al. 2011, COS Instrument Science Report 2011-02
Osten, R. A., et al. 2012, COS Instrument Science Report 2012-02
Osten, R. A. & Bostroem A., 2014, COS Technical Instrument Report 2014-03
Roman-Duval, J., et al. 2014, COS Instrument Science Report 2014-01
Roman-Duval, J., et al. 2015, COS Instrument Science Report 2015-02
de Rosa, G., et al. 2016, COS Instrument Science Report 2016-13
de Rosa, G., et al. 2017, COS Instrument Science Report 2017-10
de Rosa, G., et al. 2018, COS Instrument Science Report 2018-09
Rowlands, K. & Sankrit, R., 2022, COS Instrument Science Report 2022-08
Rowlands, K. & Sankrit, R., 2023, COS Instrument Science Report 2023-17
Rowlands, K. & Sankrit, R., 2023, COS Instrument Science Report 2024-04
Sahnou D. et al. 2016, COS Instrument Science Report 2016-08
Sana, H., et al. 2015, COS Instrument Science Report 2015-06
Sankrit, R. 2019, COS Instrument Science Report 2019-18
Sankrit, R. 2020, COS Instrument Science Report 2020-06
Sankrit, R. & Rowlands, K., 2021, COS Instrument Science Report 2021-02

Appendix A

Here we provide additional tables and figures describing the TDS observations and additional scientific testing results. Table 3 lists all the FUV TDS monitoring programs used in creating the TDSTAB since beginning of monitoring. The Cycle, Program ID, mode, target, and LP is listed. The figures include scientific testing results of various modes to quantify the improvements of the TDSTAB.

Table 3. Programs used to create new TDSTAB

Cycle	Program ID	COS Grating	Cenwave	Segment	Target	LP	
17	11897	G160M	1577	BOTH	WD1057+719	1	
			1623	BOTH	WD1057+719		
		G130M	1291	BOTH	WD0947+857		
			1327	BOTH	WD0947+857		
		G140L	1105	FUVA	WD0947+857		
			1230	BOTH	WD0947+857		
18	12424	G160M	1577	BOTH	WD1057+719	1	
			1623	BOTH	WD1057+719		
		G130M	1291	BOTH	WD0947+857		
			1327	BOTH	WD0947+857		
		G140L	1105	FUVA	WD0947+857		
			1230	BOTH	WD0947+857		
19	12715	G160M	1577	BOTH	WD1057+719	1	
				FUVA	GD71	2	
			1623	FUVB	WD0308-565	2	
				BOTH	WD1057+719	1	
			G130M	1291	FUVA	GD71	2
					FUVB	WD0308-565	2
		1327	BOTH	WD0947+857	1		
			BOTH	WD0308-565	2		
		G140L	1105	BOTH	WD0947+857	1	
				FUVA	WD0947+857	1	
			1230	FUVA	WD0308-565	2	
				BOTH	WD0947+857	1	
			1280	BOTH	WD0308-565	2	
			19	12806	G160M	1577	BOTH
FUVA	GD71	2					
1623	FUVB	WD0308-565				2	
	BOTH	WD1057+719				1	
G130M	1222 ^d	FUVA				GD71	2
		FUVB				WD0308-565	2
1291	BOTH	WD0308-565			2		
	BOTH	WD0947+857			1		
1327	BOTH	WD0308-565			2		
	BOTH	WD0947+857			1		
G140L	1105	BOTH			WD0308-565	2	
		FUVA			WD0947+857	1	
	1230 ^a	FUVA			WD0308-565	2	
		BOTH			WD0947+857	1	

Table 3. (cont'd)

Cycle	Program ID	COS Grating	Cenwave	Segment	Target	LP		
			1280 ^a	BOTH	WD0308-565	2		
20	13119	G160M	1577	FUVA	GD71	2		
				FUVB	WD0308-565	2		
			1623	FUVA	GD71	2		
				FUVB	WD0308-565	2		
		G130M	1222	BOTH	WD0308-565	2		
			1291	BOTH	WD0308-565	2		
			1327	BOTH	WD0308-565	2		
			G140L	1105	FUVA	WD0308-565	2	
1280	BOTH	WD0308-565		2				
21	13520	G160M	1577	FUVA	GD71	2		
				FUVB	WD0308-565	2		
			1623	FUVA	GD71	2		
				FUVB	WD0308-565	2		
		G130M	1055 ^{hl}	FUVA	WD0308-565	2		
			1096 ^{hl}	FUVB	GD71	2		
			1222	BOTH	WD0308-565	2		
			1291	BOTH	WD0308-565	2		
			1327	BOTH	WD0308-565	2		
			G140L	1105	FUVA	WD0308-565	2	
		1280		BOTH	WD0308-565	2		
		22	13967	G160M	1577	FUVA	GD71	2, 3
						FUVB	WD0308-565	2, 3
					1623	FUVA	GD71	2, 3
FUVB	WD0308-565					2, 3		
G130M	1055			FUVA	WD0308-565	2		
	1096			FUVB	GD71	2		
	1222			BOTH	WD0308-565	2, 3		
	1291			BOTH	WD0308-565	2, 3		
	1327			BOTH	WD0308-565	2, 3		
	G140L			1105	FUVA	WD0308-565	2, 3	
1280				BOTH	WD0308-565	2, 3		
23	14435			G160M	1577	FUVA	GD71	3
						FUVB	WD0308-565	3
					1623	FUVA	GD71	3
		FUVB	WD0308-565	3				
		G130M	1055	FUVA	WD0308-565	2		
			1096	FUVB	GD71	2		
		1222	BOTH	WD0308-565	3			

Table 3. (cont'd)

Cycle	Program ID	COS Grating	Cenwave	Segment	Target	LP
			1291	BOTH	WD0308-565	3
			1327	BOTH	WD0308-565	3
		G140L	1105	FUVA	WD0308-565	3
			1280	BOTH	WD0308-565	3
24	14854	G160M	1577	FUVA	GD71	3, 4
				FUVB	WD0308-565	3, 4
			1623	FUVA	GD71	3, 4
				FUVB	WD0308-565	3, 4
		G130M	1055	FUVA	WD0308-565	2
			1096	FUVB	GD71	2
			1222	BOTH	WD0308-565	3, 4
			1291	BOTH	WD0308-565	3, 4
			1327	BOTH	WD0308-565	3
				FUVA	WD0308-565	4
		G140L	1105	FUVA	WD0308-565	3, 4
			1280	BOTH	WD0308-565	3, 4
25	15384	G160M	1577	FUVA	GD71	4
				FUVB	WD0308-565	4
			1623	FUVA	GD71	4
				FUVB	WD0308-565	4
		G130M	1055	FUVA	WD0308-565	2
			1096	FUVB	GD71	2
			1222	BOTH	WD0308-565	4
			1291	BOTH	WD0308-565	4
			1327	FUVA	WD0308-565	4
		G140L	1105	FUVA	WD0308-565	4
			1280	BOTH	WD0308-565	4
26	15535	G160M	1533 ^c	FUVA	GD71	4
				FUVB	WD0308-565	4
			1577	FUVA	GD71	4
				FUVB	WD0308-565	4
			1623	FUVA	GD71	4
				FUVB	WD0308-565	4
		G130M	1055	FUVA	WD0308-565	2
			1096	FUVB	GD71	2
			1222	BOTH	WD0308-565	4
			1291	BOTH	WD0308-565	4
			1327	FUVA	WD0308-565	4
		G140L	800 ^c	FUVA	WD0308-565	4
			1105	FUVA	WD0308-565	4

Table 3. (cont'd)

Cycle	Program ID	COS Grating	Cenwave	Segment	Target	LP
			1280	BOTH	WD0308-565	4
27	15773	G160M	1533	FUVA	GD71	4
				FUVB	WD0308-565	4
			1577	FUVA	GD71	4
				FUVB	WD0308-565	4
			1623	FUVA	GD71	4
				FUVB	WD0308-565	4
		G130M	1055	FUVA	WD0308-565	2
			1096	FUVB	GD71	2
			1222	BOTH	WD0308-565	4
			1291	BOTH	WD0308-565	4
			1327	FUVA	WD0308-565	4
		G140L	800	FUVA	WD0308-565	4
			1105	FUVA	WD0308-565	4
			1280	BOTH	WD0308-565	4
28	16324	G160M	1533	FUVA	GD71	4
				FUVB	WD0308-565	4
			1577	FUVA	GD71	4
				FUVB	WD0308-565	4
			1623	FUVA	GD71	4
				FUVB	WD0308-565	4
		G130M	1055	FUVA	WD0308-565	2
			1096	FUVB	GD71	2
			1222	BOTH	WD0308-565	4
			1291	BOTH	WD0308-565	4, 5
			1327	FUVA	WD0308-565	4, 5
		G140L	800	FUVA	WD0308-565	4, 3
			1105	FUVA	WD0308-565	4, 3
			1280	BOTH	WD0308-565	4, 3
29	16830	G160M	1533	FUVA	GD71	4, 6
				FUVB	WD0308-565	4, 6
			1577	FUVA	GD71	4, 6
				FUVB	WD0308-565	4, 6
			1623	FUVA	GD71	4, 6
				FUVB	WD0308-565	4, 6
		G130M	1055	FUVA	WD0308-565	2
			1096	FUVB	GD71	2
			1222	BOTH	WD0308-565	4
			1291	BOTH	WD0308-565	5
			1327	FUVA	WD0308-565	5

Table 3. (cont'd)

Cycle	Program ID	COS Grating	Cenwave	Segment	Target	LP
		G140L	800	FUVA	WD0308-565	3
			1105	FUVA	WD0308-565	3
			1280	BOTH	WD0308-565	3
30	17249	G160M	1533	FUVA	GD71	6
				FUVB	WD0308-565	6
			1577	FUVA	GD71	6
				FUVB	WD0308-565	6
			1623	FUVA	GD71	6
				FUVB	WD0308-565	6
		G130M	1055	FUVA	WD0308-565	2
			1096	FUVB	GD71	2
			1222	BOTH	WD0308-565	4
			1291	BOTH	WD0308-565	5
			1327	FUVA	WD0308-565	5
		G140L	800	FUVA	WD0308-565	3
			1105	FUVA	WD0308-565	3
			1280	BOTH	WD0308-565	3
30	17251	G160M	1533	FUVA	GD71	6
				FUVB	WD0308-565	6
			1577	FUVA	GD71	6
				FUVB	WD0308-565	6
			1623	FUVA	GD71	6
				FUVB	WD0308-565	6
		G130M	1055	FUVA	WD0308-565	2
			1096	FUVB	GD71	2
			1222	BOTH	WD0308-565	4
			1291	BOTH	WD0308-565	5
			1327	FUVA	WD0308-565	5
		G140L	800	FUVA	WD0308-565	3
			1105	FUVA	WD0308-565	3
			1280	BOTH	WD0308-565	3
31	17326	G160M	1533	FUVA	GD71	6
				FUVB	WD0308-565	6
			1577	FUVA	GD71	6
				FUVB	WD0308-565	6
			1623	FUVA	GD71	6
				FUVB	WD0308-565	6
		G130M	1055	FUVA	WD0308-565	2
			1096	FUVB	GD71	2
			1222	BOTH	WD0308-565	4

Table 3. (cont'd)

Cycle	Program ID	COS Grating	Cenwave	Segment	Target	LP
			1291	BOTH	WD0308-565	5
			1327	FUVA	WD0308-565	5
		G140L	800	FUVA	WD0308-565	3
			1105	FUVA	WD0308-565	3
			1280	BOTH	WD0308-565	3
31	17328	G160M	1533	FUVA	GD71	6
				FUVB	WD0308-565	6
			1577	FUVA	GD71	6
				FUVB	WD0308-565	6
			1623	FUVA	GD71	6
				FUVB	WD0308-565	6
		G130M	1055	FUVA	WD0308-565	2
			1096	FUVB	GD71	2
			1222	BOTH	WD0308-565	4
			1291	BOTH	WD0308-565	5
			1327	FUVA	WD0308-565	5
		G140L	800	FUVA	WD0308-565	3
			1105	FUVA	WD0308-565	3
			1280	BOTH	WD0308-565	3

^aG140L/1230 was replaced by G140L/1280 after LP1.

^bBlue mode data between 19 September 2012 and 20 October 2013 were removed due to a known bug.

^cNew cenwaves enabled for G130M and G140L at start of LP4.

^dNew cenwaves enabled for G130M at start of LP2.

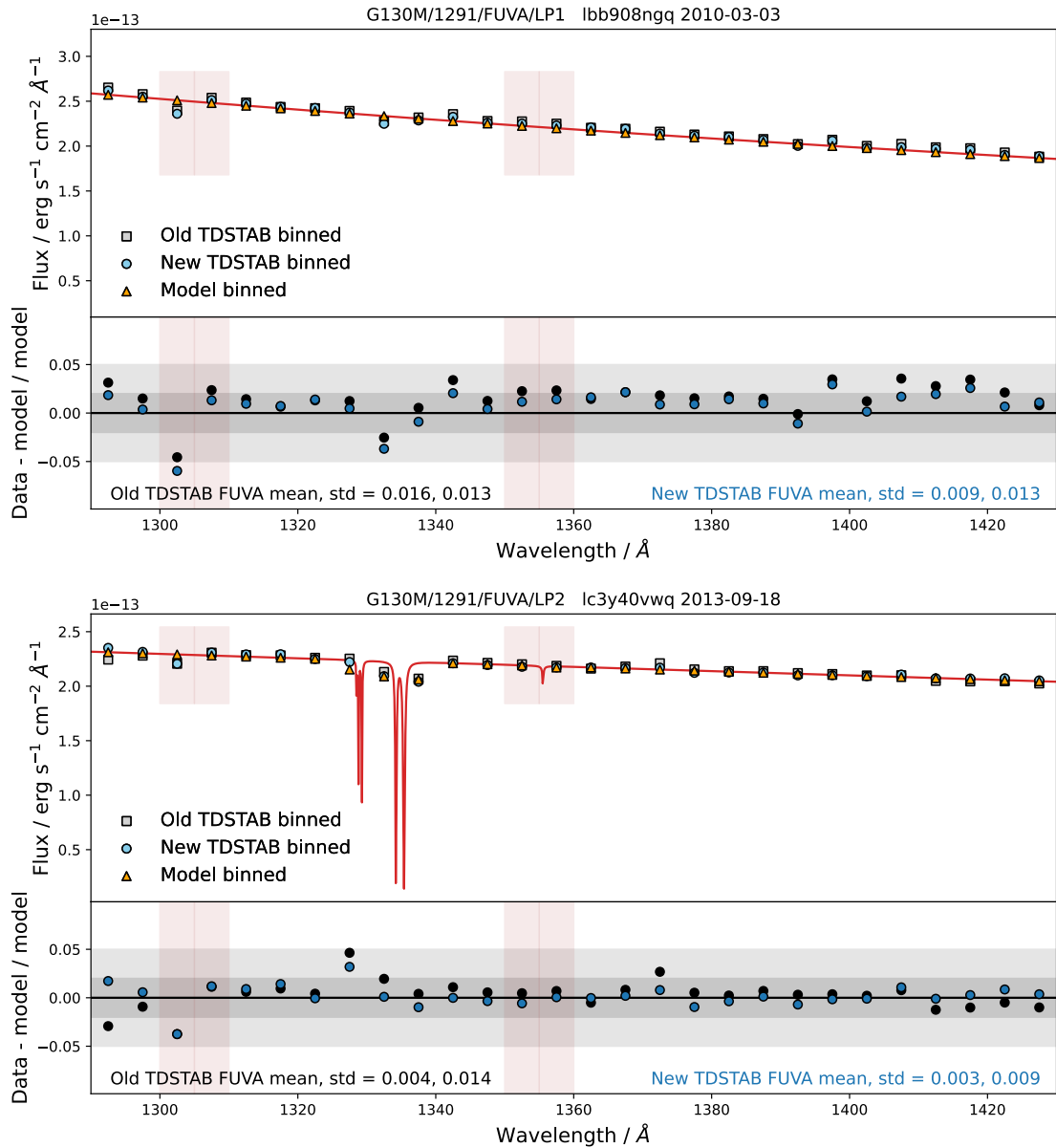


Figure 4. Fluxes and residuals for example TDS monitoring observations from programs 11897 and 13119 for G130M/1291/FUVA at LP1 and LP2 used in the creation of the TDSTAB. The old (black, grey) and new (blue) TDSTAB are used and the calibrated data is compared to the CALSPEC model fluxes (red) for WD0947+857 (top) and WD0308-565 (bottom). Residuals between the data and model show that there is no systematic offset as a function of wavelength and depict improvements at all LPs. The binned residuals are typically within the 5% absolute flux calibration goals. The dark and light grey shaded regions show the 2% and 5% flux residual regions.

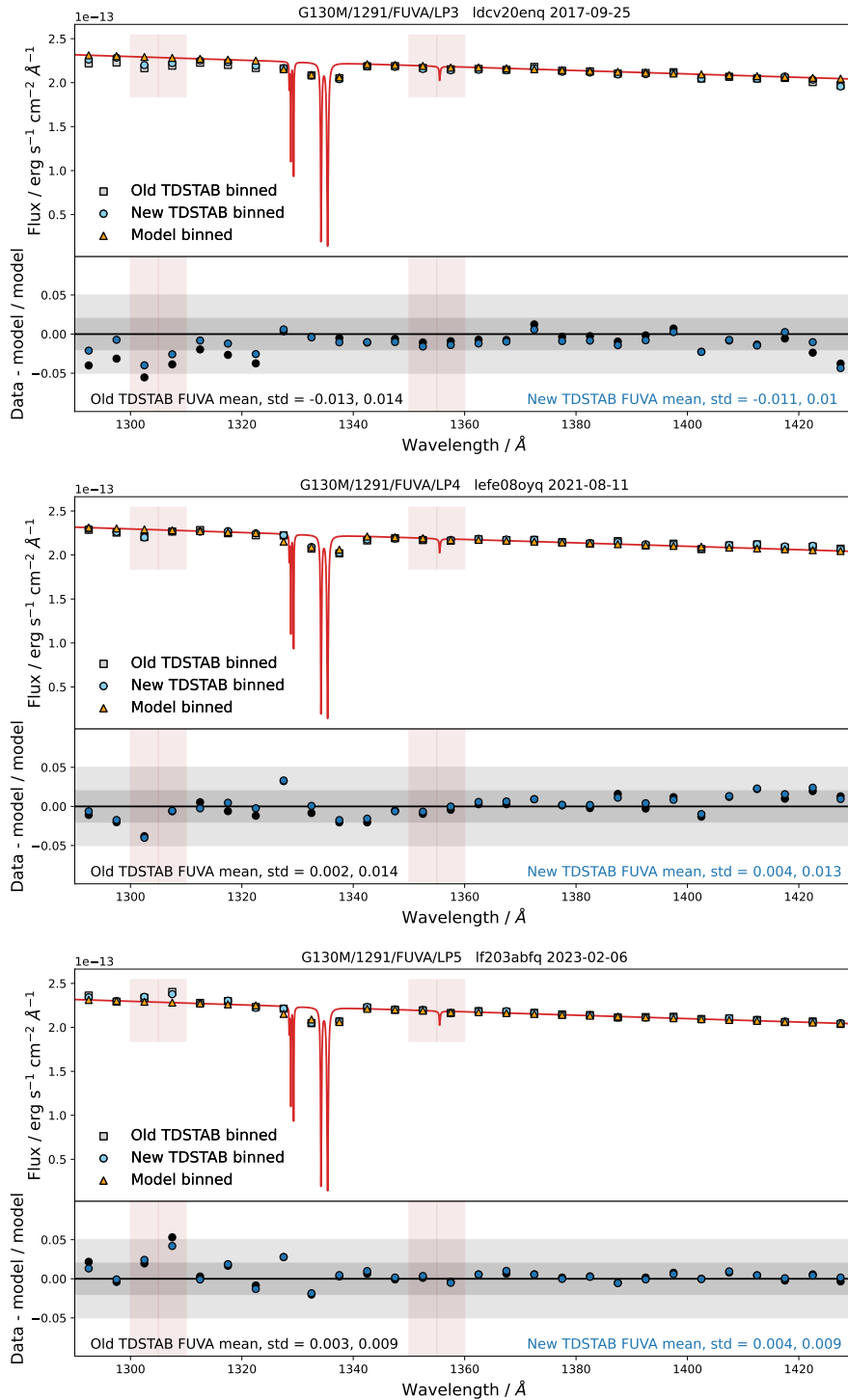


Figure 5. Fluxes and residuals for example TDS monitoring observations from programs 14854, 16324 and 17249 for G130M/1291/FUVA at LP3, LP4, and LP5 used in the creation of the TDSTAB. The old (black, grey) and new (blue) TDSTAB are used and the calibrated data is compared to the CALSPEC model fluxes (red) for WD0308-565. See Figure 4 for additional description.

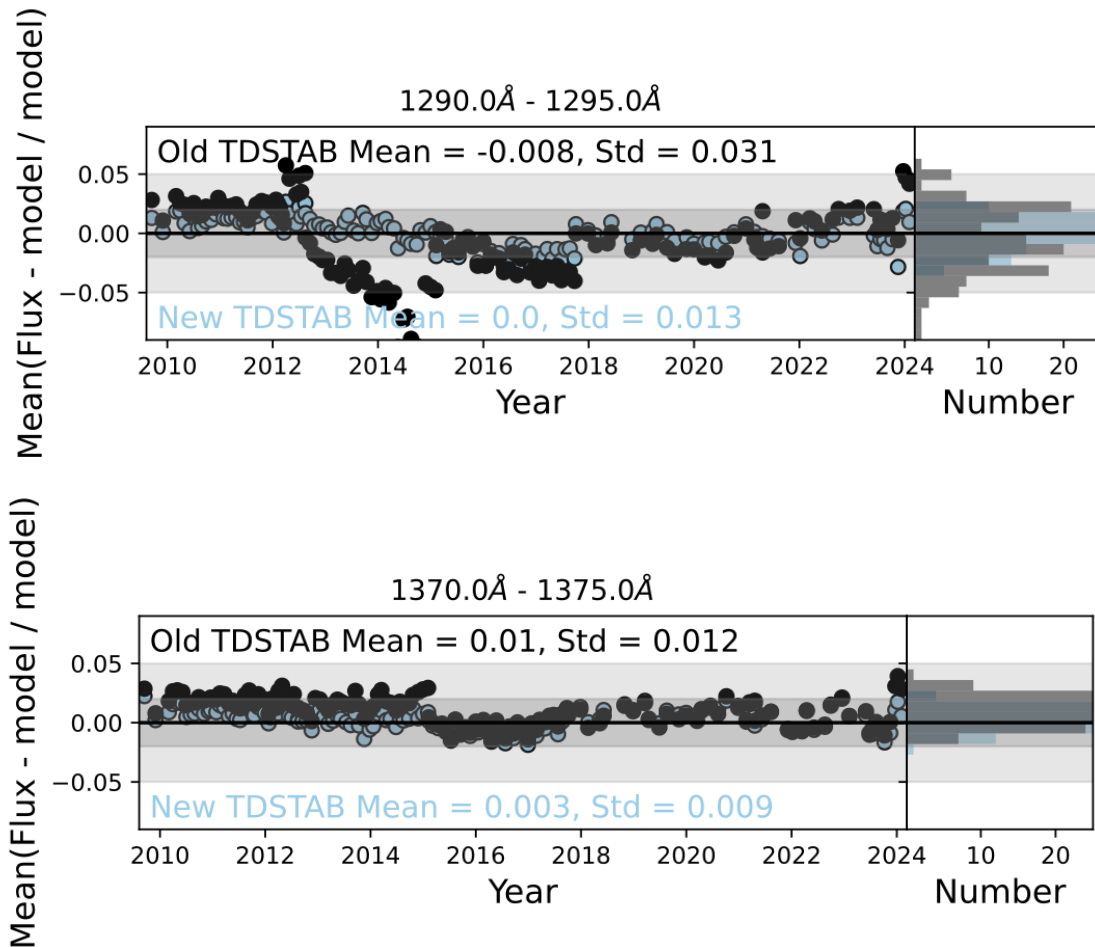


Figure 6. Example mean flux residuals as a function of time, comparing the flux from G130M/1291/FUVA data calibrated with the old TDSTAB (black) and the new TDSTAB (blue) and compared with the WD0947+857 and WD0308-565 CALSPEC models (wd0947_857_mod_003.fits, wd0308_565_mod_006.fits, spectra derived from Bohlin et al. 2014 and Bohlin et al. 2020). The panels show data in 5 Å bins for segment FUVA of the blue edge (top) and the center (bottom) of cenwave 1291. The dark and light grey shaded regions show the 2% and 5% flux residual regions.

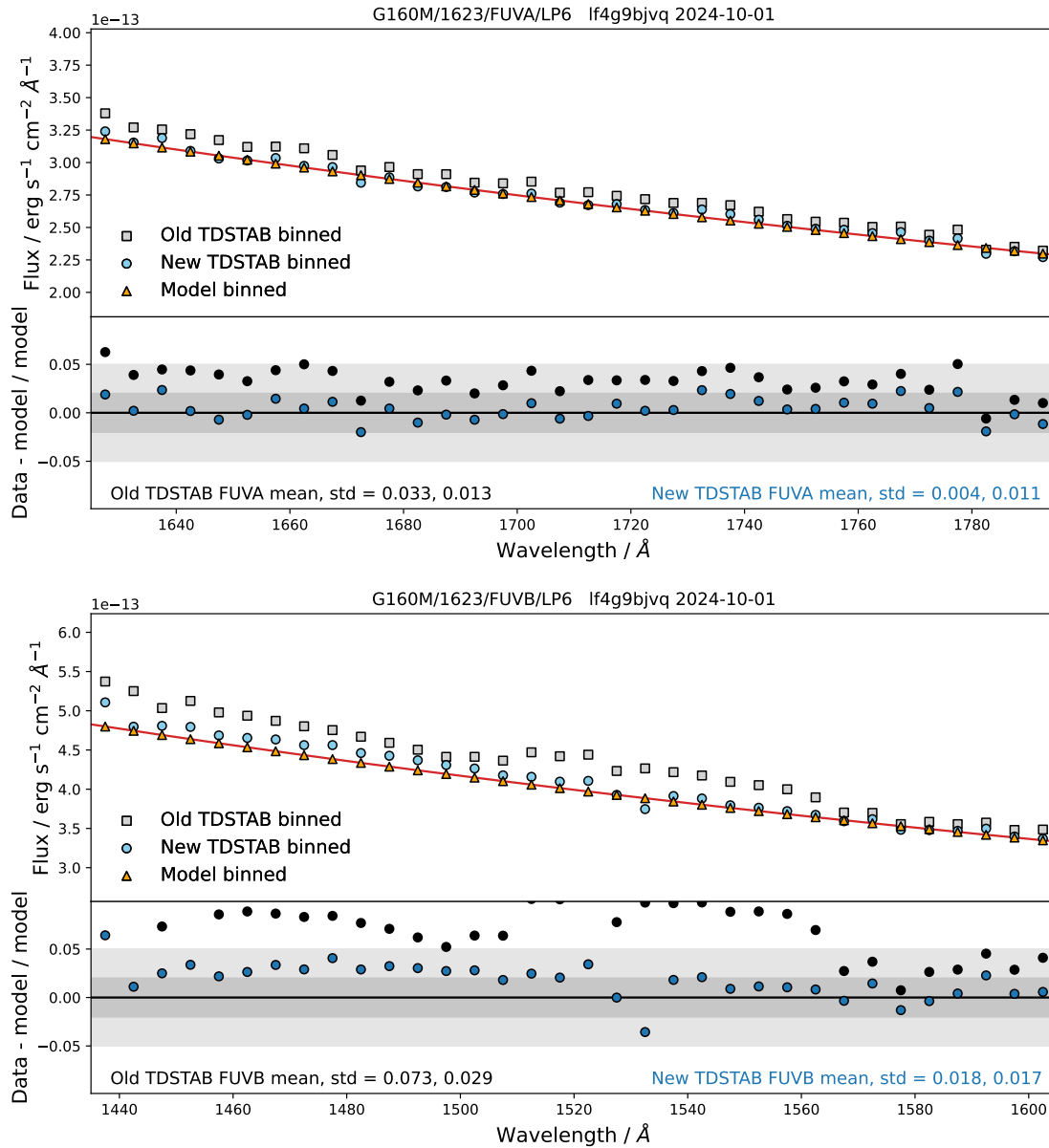


Figure 7. Fluxes and residuals for example TDS monitoring observations G160M/1623/FUVA and FUVB at LP6 not included in the TDSTAB creation as a test for the new TDSTAB. The old (black, grey) and new (blue) TDSTAB are used and the calibrated data is compared to the CALSPEC model flux (red) for WD1057+719. Residuals between the data and model show that there is no systematic offset as a function of wavelength and depict improvements at times the HV was raised due to the inclusion of the HVDS. The binned residuals are typically within the 5% absolute flux calibration goals. The dark and light grey shaded regions show the 2% and 5% flux residual regions.

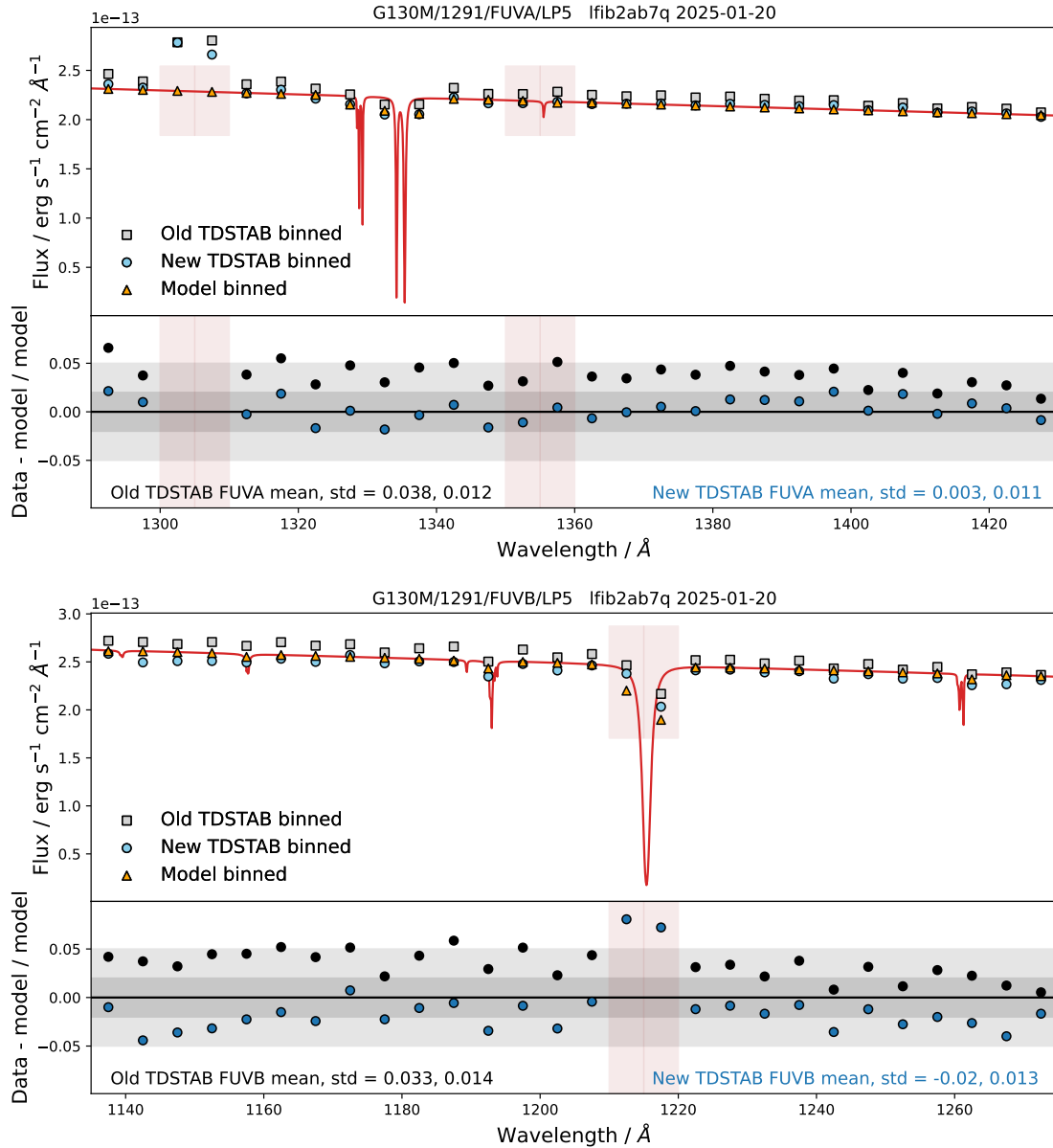


Figure 8. Fluxes and residuals for example TDS monitoring observations G130M/1291/FUVA and FUVB at LP5 not included in the TDSTAB creation. The old (black, grey) and new (blue) TDSTAB are used and the calibrated data is compared to the CALSPEC model flux (red) for WD0308-575. Residuals between the data and model show that there is no systematic offset as a function of wavelength and depict improvements at times the HV was raised due to the inclusion of the HVDS. The binned residuals are typically within the 5% absolute flux calibration goals. The dark and light grey shaded regions show the 2% and 5% flux residual regions.

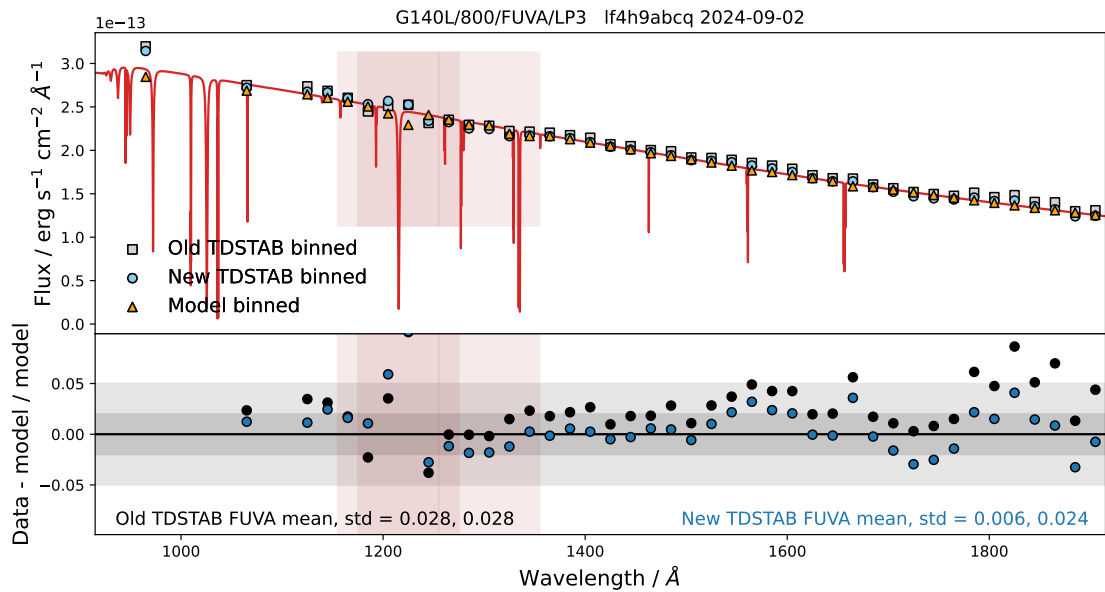


Figure 9. Fluxes and residuals for example TDS monitoring observations G140L/800/FUVA at LP3 not included in the TDSTAB creation. The old (black, grey) and new (blue) TDSTAB are used and the calibrated data is compared to the CALSPEC model flux (red) for WD0308-575. Residuals between the data and the model indicate no systematic offset as a function of wavelength. The binned residuals are typically within the 5% absolute flux calibration goals. The dark and light grey shaded regions show the 2% and 5% flux residual regions.

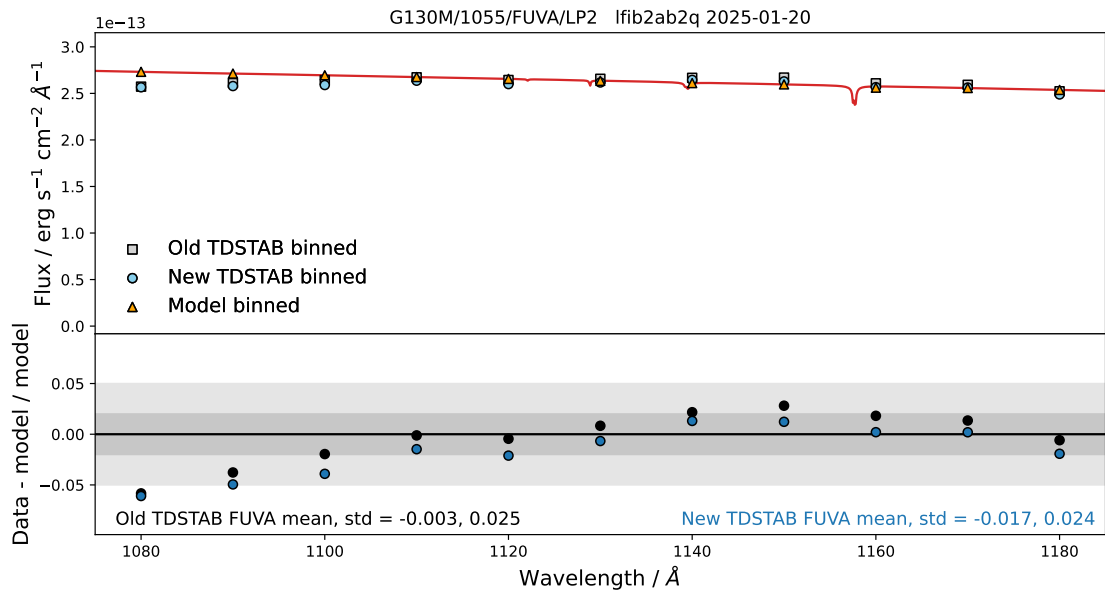


Figure 10. Fluxes and residuals for example TDS monitoring observations blue modes G130M/1055/FUVA at LP2 not included in the TDSTAB creation. The old (black, grey) and new (blue) TDSTAB are used and the calibrated data is compared to the CALSPEC model flux (red) for WD0308-575. Residuals between the data and model show that there is no systematic offset as a function of wavelength. The binned residuals are typically within the 5% absolute flux calibration goals. The dark and light grey shaded regions show the 2% and 5% flux residual regions.